

# The Hubble Constant from Gravitational Lens Time Delays

CHRISTOPHER S. KOCHANEK  
*Harvard-Smithsonian Center for Astrophysics*

PAUL L. SCHECHTER  
*Massachusetts Institute of Technology*

---

## Abstract

There are now 10 firm time delay measurements in gravitational lenses. The physics of time delays is well understood, and the only important variable for interpreting the time delays to determine  $H_0$  is the mean surface mass density  $\langle\kappa\rangle$  (in units of the critical density for gravitational lensing) of the lens galaxy at the radius of the lensed images. More centrally concentrated mass distributions with lower  $\langle\kappa\rangle$  predict higher Hubble constants, with  $H_0 \propto 1 - \langle\kappa\rangle$  to lowest order. While we cannot determine  $\langle\kappa\rangle$  directly given the available data on the current time delay lenses, we find  $H_0 = 48 \pm 3 \text{ km s}^{-1} \text{ Mpc}^{-1}$  for the isothermal (flat rotation curve) models, which are our best present estimate for the mass distributions of the lens galaxies. Only if we eliminate the dark matter halo of the lenses and use a constant mass-to-light ratio ( $M/L$ ) model to find  $H_0 = 71 \pm 3 \text{ km s}^{-1} \text{ Mpc}^{-1}$  is the result consistent with local estimates. Measurements of time delays in better-constrained systems or observations to obtain new constraints on the current systems provide a clear path to eliminating the  $\langle\kappa\rangle$  degeneracy and making estimates of  $H_0$  with smaller uncertainties than are possible locally. Independent of the value of  $H_0$ , the time delay lenses provide a new and unique probe of the dark matter distributions of galaxies and clusters because they measure the total (light + dark) matter surface density.

## 1.1 Introduction

Fifteen years prior to their discovery in 1979, Refsdal (1964) outlined how gravitationally lensed quasars might be used to determine the Hubble constant. Astronomers have spent the quarter century since their discovery working out the difficult details not considered in Refsdal's seminal papers.

The difficulties encountered fall into two broad categories — measurement and modeling. Time delays can be hard to measure if the fluxes of the images do not vary, or if the images are faint, or if they lie very close to each other. Modeling gravitational potentials with a small number of constraints is likewise difficult, either because the lens geometry is complex or because the data poorly constrain the most important aspects of the gravitational potential. We will argue that these difficulties are surmountable, both in principle and in practice, and that an effort considerably smaller than that of the *HST* Hubble Constant Key Project will yield a considerably smaller uncertainty in the Hubble constant,  $H_0$ .

While the number of systems with measured time delays is small, their interpretation im-

plies a value for  $H_0$ , which, given our current understanding of the dark matter distributions of galaxies, is formally inconsistent with that obtained using Cepheids. The Key Project value of  $H_0 = 72 \pm 8 \text{ km s}^{-1} \text{ Mpc}^{-1}$  (Freedman et al. 2001) is consistent with the lens data only if the lens galaxies have significantly less dark matter than is expected theoretically or has been measured for other early-type galaxies. While it is premature to argue for replacing the local estimates, we hope to persuade the astronomical community that the time delay result deserves both careful attention and further study.

Interpreting time delays requires a model for the gravitational potential of the lens, and in most cases the uncertainties in the model dominate the uncertainty in  $H_0$ . Thus, the main focus of this review will be to explain the dependence of time delays on gravitational potentials. We start in §1.2 by introducing the time delay method and illustrating the physics of time delays with a series of simple models. In §1.3 we review a general mathematical theory of time delays to show that, for most lenses, the only important parameter of the model is the mean surface density of the lens at the radius of the images. In §1.4 we discuss the effects of the environment of the lens on time delays. We review the data on the time delay lenses in §1.5 and their implications for the Hubble constant and dark matter in early-type galaxies in §1.6. The present time delay lenses have a degeneracy between  $H_0$  and the amount of dark matter, so in §1.7 we outline several approaches that can eliminate the degeneracy. Finally, in §1.8 we discuss the future of time delays. Unless otherwise stated, we assume a flat,  $\Omega_m = 0.3$ ,  $\Omega_\Lambda = 0.7$  cosmological model.

## 1.2 Time Delay Basics

The observations of gravitationally lensed quasars are best understood in light of Fermat's principle (e.g., Blandford & Narayan 1986). Intervening mass between a source and an observer introduces an effective index of refraction, thereby increasing the light-travel time. The competition between this Shapiro delay from the gravitational field and the geometric delay due to bending the ray paths leads to the formation of multiple images at the stationary points (minima, maxima, and saddle points) of the travel time (for more complete reviews, see Narayan & Bartelmann 1999 or Schneider, Ehlers, & Falco 1992).

As with glass optics, there is a thin-lens approximation that applies when the optics are small compared to the distances to the source and the observer. In this approximation, we need only the effective potential,  $\psi(\vec{x}) = (2/c^2)(D_{ls}/D_s) \int dz\phi$ , found by integrating the 3D potential  $\phi$  along the line of sight. The light-travel time is

$$\tau(\vec{x}) = \left[ \frac{1+z_l}{c} \right] \left[ \frac{D_l D_s}{D_{ls}} \right] \left[ \frac{1}{2} (\vec{x} - \vec{\beta})^2 - \psi(\vec{x}) \right], \quad (1.1)$$

where  $\vec{x} = (x, y) = R(\cos\theta, \sin\theta)$  and  $\vec{\beta}$  are the angular positions of the image and the source,  $\psi(\vec{x})$  is the effective potential,  $(\vec{x} - \vec{\beta})^2/2$  is the geometric delay in the small-angle approximation,  $z_l$  is the lens redshift, and  $D_l$ ,  $D_s$ , and  $D_{ls}$  are angular-diameter distances to the lens, to the source, and from the lens to the source, respectively. The only dimensioned quantity in the travel time is a factor of  $H_0^{-1} \simeq 10h^{-1} \text{ Gyr}$  arising from the  $H_0^{-1}$  scaling of the angular-diameter distances.

We observe the images at the extrema of the time delay function, which we find by setting the gradients with respect to the image positions equal to zero,  $\vec{\nabla}_{\vec{x}}\tau = 0$ , and finding all the stationary points  $(\vec{x}_A, \vec{x}_B, \dots)$  associated with a given source position  $\vec{\beta}$ . The local magnifica-

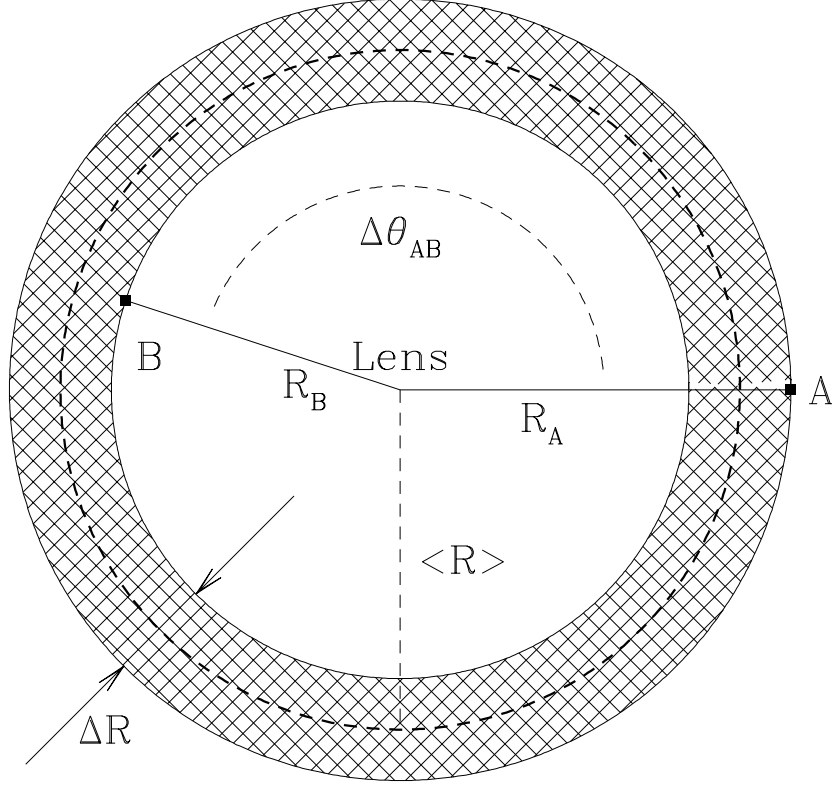


Fig. 1.1. Schematic diagram of a two-image time delay lens. The lens lies at the origin, with two images A and B at radii  $R_A$  and  $R_B$  from the lens center. The images define an annulus of average radius  $\langle R \rangle = (R_A + R_B)/2$  and width  $\Delta R = R_A - R_B$ , and the images subtend an angle  $\Delta\theta_{AB}$  relative to the lens center. For a circular lens  $\Delta\theta_{AB} = 180^\circ$  by symmetry.

tion of an image is determined by the magnification tensor  $M_{ij}$ , whose inverse is determined by the second derivatives of the time delay function,

$$M_{ij}^{-1} = \vec{\nabla}_x \vec{\nabla}_x \tau(\vec{x}) = \begin{pmatrix} 1 - \kappa - \gamma \cos 2\theta_\gamma & \gamma \sin 2\theta_\gamma \\ \gamma \sin 2\theta_\gamma & 1 - \kappa + \gamma \cos 2\theta_\gamma \end{pmatrix}, \quad (1.2)$$

where the convergence  $\kappa = \Sigma/\Sigma_c$  is the local surface density in units of the critical surface density  $\Sigma_c = c^2 D_s / 4\pi G D_l D_{ls}$ , and  $\gamma$  and  $\theta_\gamma$  define the local shear field and its orientation. The determinant of the magnification tensor is the net magnification of the image, but it is a signed quantity depending on whether the image has positive (maxima, minima) or negative (saddle points) parity.

C. S. Kochanek and P. L. Schechter

A simple but surprisingly realistic starting point for modeling lens potentials is the singular isothermal sphere (the SIS model) in which the lens potential is simply

$$\psi(\vec{x}) = bR, \quad \text{where} \quad b = 4\pi \frac{D_{ls}}{D_s} \frac{\sigma^2}{c^2} = 1''.45 \left( \frac{\sigma}{225 \text{ km s}^{-1}} \right)^2 \frac{D_{ls}}{D_s} \quad (1.3)$$

is a deflection scale determined by geometry and  $\sigma$  is the 1D velocity dispersion of the lens galaxy. For  $|\vec{\beta}| < b$ , the SIS lens produces two colinear images at radii  $R_A = |\vec{\beta}| + b$  and  $R_B = b - |\vec{\beta}|$  on opposite sides of the lens galaxy (as in Fig. 1.1 but with  $\Delta\theta_{AB} = 180^\circ$ ).<sup>\*</sup> The A image is a minimum of the time delay and leads the saddle point, B, with a time delay difference of

$$\Delta t_{SIS} = \tau_B - \tau_A = \frac{1}{2} \left[ \frac{1+z_l}{c} \right] \left[ \frac{D_l D_s}{D_{ls}} \right] (R_A^2 - R_B^2). \quad (1.4)$$

Typical time delay differences of months or years are the consequence of multiplying the  $\sim 10h^{-1}$  Gyr total propagation times by the square of a very small angle ( $b \approx 3 \times 10^{-6}$  radians so,  $R_A^2 \approx 10^{-11}$ ). The SIS model suggests that lens time delay measurements reduce the determination of the Hubble constant to a problem of differential astrometry. This is almost correct, but we have made two idealizations in using the SIS model.

The first idealization was to ignore deviations of the radial (monopole) density profile from that of an SIS with density  $\rho \propto r^{-2}$ , surface density  $\Sigma \propto R^{-1}$ , and a flat rotation curve. The SIS is a special case of a power-law monopole with lens potential

$$\psi(\vec{x}) = \frac{b^2}{(3-\eta)} \left( \frac{R}{b} \right)^{3-\eta}, \quad (1.5)$$

corresponding to a (3D) density distribution with density  $\rho \propto r^{-\eta}$ , surface density  $\Sigma \propto R^{1-\eta}$ , and rotation curve  $v_c \propto r^{(2-\eta)/2}$ . For  $\eta = 2$  we recover the SIS model, and the normalization is chosen so that the scale  $b$  is always the Einstein ring radius. Models with smaller (larger)  $\eta$  have less (more) centrally concentrated mass distributions and have rising (falling) rotation curves. The limit  $\eta \rightarrow 3$  approaches the potential of a point mass. By adjusting the scale  $b$  and the source position  $|\vec{\beta}|$ , we can fit the observed positions of two images at radii  $R_A$  and  $R_B$  on opposite sides ( $\Delta\theta_{AB} = 180^\circ$ ) of the lens for any value of  $\eta$ .<sup>†</sup> The expression for the time delay difference can be well approximated by (Witt, Mao, & Keeton 2000; Kochanek 2002)

$$\Delta t(\eta) = \tau_B - \tau_A \simeq (\eta - 1) \Delta t_{SIS} \left[ 1 - \frac{(2-\eta)^2}{12} \left( \frac{\Delta R}{\langle R \rangle} \right)^2 \dots \right], \quad (1.6)$$

where  $\langle R \rangle = (R_A + R_B)/2 \simeq b$  and  $\Delta R = R_A - R_B$  (see Fig. 1.1). While the expansion assumes  $\Delta R/\langle R \rangle$  (or  $|\vec{\beta}|$ ) is small, we can usually ignore the higher-order terms. There are two important lessons from this model.

<sup>\*</sup> The deflections produced by the SIS lens are constant,  $|\vec{x} - \vec{\beta}| = b$ , so the total image separation is always  $2b$ . The outer image is brighter than the inner image, with signed magnifications  $M_A^{-1} = 1 - b/R_A > 0$  (a positive parity minimum) and  $M_B^{-1} = 1 - b/R_B < 0$  (a negative parity saddle point). The model parameters,  $b = (R_A + R_B)/2 = \langle R \rangle$  and  $|\vec{\beta}| = (R_A - R_B)/2 = \Delta R/2$ , can be determined uniquely from the image positions.

<sup>†</sup> In theory we have one additional constraint because the image flux ratio measures the magnification ratio,  $f_A/f_B = |M_A|/|M_B|$ , and the magnification ratio depends on  $\eta$ . Unfortunately, the systematic errors created by milli- and microlensing make it difficult to use flux ratios as model constraints (see §1.5).

C. S. Kochanek and P. L. Schechter

- (1) Image astrometry of simple two-image and four-image lenses generally cannot constrain the radial mass distribution of the lens.
- (2) More centrally concentrated mass distributions (larger  $\eta$ ) predict longer time delays, resulting in a larger Hubble constant for a given time delay measurement.

These problems, which we will address from a different perspective in §1.3, are the cause of the uncertainties in estimates of  $H_0$  from time delays.

The second idealization was to ignore deviations from circular symmetry due to either the ellipticity of the lens galaxy or the local tidal gravity field from nearby objects. A very nice analytic example of a lens with angular structure is a singular isothermal model with *arbitrary* angular structure, where the effective potential is  $\psi = bRF(\theta)$ , and  $F(\theta)$  is an arbitrary function. The model family includes the most common lens model, the singular isothermal ellipsoid (SIE). The time delays for this model family are simply  $\Delta t_{SIS}$ , *independent of the angular structure of the lens* (Witt et al. 2000)! This result, while attractive, does not hold in general, and we will require the results of §1.3 to understand the effects of angular structure in the potential.

### 1.3 Understanding Time Delays: A General Theory

The need to model the gravitational potential of the lens is the aspect of interpreting time delays that creates the greatest suspicion. The most extreme view is that it renders the project “hopeless” because we will never be able to guarantee that the models encompass the degrees of freedom needed to capture all the systematic uncertainties. In order to address these fears we must show that we understand the specific properties of the gravitational potential determining time delays and then ensure that our parameterized models include these degrees of freedom.

The examples we considered in §1.2 illustrate the basic physics of time delays, but an extensive catalog of (non)parametric models demonstrating the same properties may not be convincing to the skeptic. We will instead show, using standard mathematical expansions of the potential, which properties of the lens galaxy are required to understand time delays with accuracies of a few percent. While we can understand the results of all models for the time delays of gravitational lenses based on this simple theory, full numerical models should probably be used for most detailed, quantitative analyses. Fortunately, there are publically available programs for both the parametric and nonparametric approaches.\* Our analysis uses the geometry of the schematic lens shown in Figure 1.1. The two images define an annulus bounded by their radii,  $R_A$  and  $R_B$ , and with an interior region for  $R < R_B$  and an exterior region for  $R > R_A$ .

The key to understanding time delays comes from Gorenstein, Falco, & Shapiro (1988; see also Saha 2000), who showed that the time delay of a circular lens depends only on the image positions and the *surface density*  $\kappa(R)$  *in the annulus between the images*. The mass of the interior region is implicit in the image positions and accurately determined by the astrometry. From Gauss’ law, we know that the radial distribution of the mass in the interior region and the amount or distribution of mass in the exterior region is irrelevant. A useful approximation is to assume that the surface density in the annulus can be *locally*

\* The *gravlens* and *lensmodel* (Keeton 2003, cfa-www.harvard.edu/~castles) packages include a very broad range of parametric models for the mass distributions of lenses, and the *PixelLens* package (Williams & Saha 2000, ankh-morpork.maths.qmw.ac.uk/~saha/astron/lens/pix/) implements a nonparametric approach.

C. S. Kochanek and P. L. Schechter

approximated by a power law  $\kappa \propto R^{1-\eta}$  and that the mean surface density in the annulus is  $\langle \kappa \rangle = \langle \Sigma \rangle / \Sigma_c$ . The time delay between the images is (Kochanek 2002)

$$\Delta t = 2\Delta t_{SIS} \left[ 1 - \langle \kappa \rangle - \frac{1-\eta\langle \kappa \rangle}{12} \left( \frac{\Delta R}{\langle R \rangle} \right)^2 + O \left( \left( \frac{\Delta R}{\langle R \rangle} \right)^4 \right) \right]. \quad (1.7)$$

Thus, the time delay is largely determined by the average density  $\langle \kappa \rangle$ , with only modest corrections from the local shape of the surface density distribution even when  $\Delta R / \langle R \rangle \simeq 1$ . For example, the second-order expansion is exact for an SIS lens ( $\langle \kappa \rangle = 1/2$ ,  $\eta = 2$ ) and reproduces the time delay of a point mass lens ( $\langle \kappa \rangle = 0$ ) to better than 1% even when  $\Delta R / \langle R \rangle = 1$ . This local model also explains the time delay scalings of the global power-law models we discussed in §1.2. A  $\rho \propto r^{-\eta}$  global power law has surface density  $\langle \kappa \rangle = (3-\eta)/2$  near the Einstein ring, so the leading term of the time delay is  $\Delta t = 2\Delta t_{SIS}(1 - \langle \kappa \rangle) = (\eta - 1)\Delta t_{SIS}$ , just as in Equation (1.6).

- The time delay is not determined by the global structure of the radial density profile but rather by the surface density near the Einstein ring.

Gorenstein et al. (1988) considered only circular lenses, but a multipole expansion allows us to understand the role of angular structure (Kochanek 2002). An estimate to the same order as in Equation (1.7) requires only the quadrupole moments of the regions interior and exterior to the annulus, provided the strengths of the higher-order multipoles of the potential have the same order of magnitude as for an ellipsoidal density distribution.\* This approximation can fail for the lenses in clusters (see §1.4). The complete expansion for  $\Delta t$  when the two quadrupole moments have independent amplitudes and orientations is not very informative. However, the leading term of the expansion when the two quadrupole moments are aligned illustrates the role of angular structure. Given an exterior quadrupole (i.e., an external shear) of amplitude  $\gamma_{ext}$  and an interior quadrupole of amplitude  $\gamma_{int}$  sharing a common axis  $\theta_\gamma$ , the quadrupole potential is

$$\psi_2 = \frac{1}{2} \left( \gamma_{ext} R^2 + \gamma_{int} \frac{\langle R \rangle^4}{R^2} \right) \cos 2(\theta - \theta_\gamma) \quad (1.8)$$

if we define the amplitudes at radius  $\langle R \rangle$ . For images at positions  $R_A(\cos \theta_A, \sin \theta_A)$  and  $R_B(\cos \theta_B, \sin \theta_B)$  relative to the lens galaxy (see Fig. 1.1), the leading term of the time delay is

$$\Delta t \simeq 2\Delta t_{SIS}(1 - \langle \kappa \rangle) \frac{\sin^2(\Delta\theta_{AB}/2)}{1 - 4f_{int} \cos^2(\Delta\theta_{AB}/2)}, \quad (1.9)$$

where  $\Delta\theta_{AB} = \theta_A - \theta_B$  and  $f_{int} = \gamma_{int} / (\gamma_{ext} + \gamma_{int})$  is the fraction of the quadrupole due to the interior quadrupole moment  $\gamma_{int}$ . We need not worry about the possibility of a singular denominator — successful global models of the lens do not allow such configurations.

\* If the quadrupole potential,  $\psi_2 \propto \cos 2\theta$ , has dimensionless amplitude  $\epsilon_2$ , then it produces ray deflections of order  $O(\epsilon_2 b)$  at the Einstein ring of the lens. In a four-image lens the quadrupole deflections are comparable to the thickness of the annulus, so  $\epsilon_2 \simeq \Delta R / \langle R \rangle$ . In a two-image lens they are smaller than the thickness of the annulus, so  $\epsilon_2 \lesssim \Delta R / \langle R \rangle$ . For an ellipsoidal density distribution, the  $\cos(2m\theta)$  multipole amplitude scales as  $\epsilon_{2m} \sim \epsilon_2^m \lesssim (\Delta R / \langle R \rangle)^m$ . This allows us to ignore the quadrupole density distribution in the annulus and all higher-order multipoles. It is important to remember that potentials are much rounder than surface densities [with relative amplitudes for a  $\cos(m\theta)$  multipole of roughly  $m^{-2}:m^{-1}:1$  for potentials:deflections:densities], so the multipoles relevant to time delays converge rapidly even for very flat surface density distributions.

A two-image lens has too few astrometric constraints to fully constrain a model with independent, misaligned internal and external quadrupoles. Fortunately, when the lensed images lie on opposite sides of the lens galaxy ( $\Delta\theta_{AB} \simeq \pi + \delta$ ,  $|\delta| \ll 1$ ), the time delay becomes insensitive to the quadrupole structure. Provided the angular deflections are smaller than the radial deflections ( $|\delta| \langle R \rangle \lesssim \Delta R$ ), the leading term of the time delay reduces to the result for a circular lens,  $\Delta t \simeq 2\Delta t_{SIS}(1 - \langle \kappa \rangle)$ . There is, however, one limiting case to remember. If the images and the lens are colinear, as in a spherical lens, the component of the shear aligned with the separation vector acts like a contribution to the convergence. In most lenses this would be a modest additional uncertainty — in the typical lens these shears must be small, the sign of the effect should be nearly random, and it is only a true degeneracy in the limit that everything is colinear.

A four-image lens has more astrometric constraints and can constrain a model with independent, misaligned internal and external quadrupoles. The quadrupole moments of the observed lenses are dominated by external shear, with  $f_{int} \lesssim 1/4$  unless there is more than one lens galaxy inside the Einstein ring. The ability of the astrometry to constrain  $f_{int}$  is important because the delays depend strongly on  $f_{int}$  when the images do not lie on opposite sides of the galaxy. If external shears dominate,  $f_{int} \simeq 0$  and the leading term of the delay becomes  $\Delta t \simeq 2\Delta t_{SIS}(1 - \langle \kappa \rangle) \sin^2 \Delta\theta_{AB}/2$ . If the model is isothermal, like the  $\psi = rF(\theta)$  models we considered in §1.2, then  $f_{int} = 1/4$  and we again find that the delay is independent of the angle, with  $\Delta t \simeq 2\Delta t_{SIS}(1 - \langle \kappa \rangle)$ . The time delay ratios in a four-image lens are largely determined by the angular structure and provide a check of the potential model.

In summary, if we want to understand time delays to an accuracy competitive with studies of the local distance scale (5%–10%), the only important variable is the surface density  $\langle \kappa \rangle$  of the lens in the annulus between the images. When models based on the same data for the time delay and the image positions predict different values for  $H_0$ , the differences can always be understood as the consequence of different choices for  $\langle \kappa \rangle$ . In parametric models  $\langle \kappa \rangle$  is adjusted by changing the central concentration of the lens (i.e., like  $\eta$  in the global power-law models), and in the nonparametric models of Williams & Saha (2000) it is adjusted directly. The expansion models of Zhao & Qin (2003a,b) mix aspects of both approaches.

#### 1.4 Lenses Within Clusters

Most galaxies are not isolated, and many early-type lens galaxies are members of groups or clusters, so we need to consider the effects of the local environment on the time delays. Weak perturbations are easily understood since they will simply be additional contributions to the surface density ( $\langle \kappa \rangle$ ) and the external shear/quadrupole ( $\gamma_{ext}$ ) we discussed in §1.3. In this section we focus on the consequences of large perturbations.

As a first approximation we can assume that a nearby cluster (or galaxy) can be modeled by an SIS potential,  $\Psi_c(\vec{x}) = B|\vec{x} - \vec{x}_c|$ , where  $B$  is the Einstein radius of the cluster and  $\vec{x}_c = R_c(\cos\theta_c, \sin\theta_c)$  is the position of the cluster relative to the primary lens. We can understand its effects by expanding the potential as a series in  $R/R_c$ , dropping constant and linear terms that have no observable consequences, to find that

$$\Psi_c \simeq \frac{1}{4} \frac{B}{R_c} R^2 - \frac{1}{4} \frac{B}{R_c} R^2 \cos 2(\theta - \theta_c) + O\left(\frac{B}{R_c^2} R^3\right). \quad (1.10)$$

The first term has the form  $(1/2)\kappa_c R^2$ , which is the potential of a uniform sheet whose surface density  $\kappa_c = B/2R_c$  is that of the cluster at the lens center. The second term has the

form  $(1/2)\gamma_c R^2 \cos 2(\theta - \theta_c)$ , which is the (external) tidal shear  $\gamma_c = B/2R_c$  that would be produced by putting all the cluster mass inside a ring of radius  $R_c$  at the cluster center. All realistic lens models need to incorporate a tidal shear term due to objects near the lens or along the line of sight (Keeton, Kochanek, & Seljak 1997), but as we discussed in §1.3 the shear does not lead to significant ambiguities in the time delay estimates. Usually the local shear cannot be associated with a particular object unless it is quite strong ( $\gamma_c \approx 0.1$ ).\*

The problems with nearby objects arise when the convergence  $\kappa_c$  becomes large because of a global degeneracy known as the *mass-sheet degeneracy* (Falco, Gorenstein, & Shapiro 1985). If we have a model predicting a time delay  $\Delta t_0$  and then add a sheet of constant surface density  $\kappa_c$ , then the time delay is changed to  $(1 - \kappa_c)\Delta t_0$  without changing the image positions, flux ratios, or time delay ratios. Its effects can be understood from §1.3 as a contribution to the annular surface density with  $\langle \kappa \rangle = \kappa_c$  and  $\eta = 1$ . The parameters of the lens, in particular the mass scale  $b$ , are also rescaled by factors of  $1 - \kappa_c$ , so the degeneracy can be broken if there is an independent mass estimate for either the cluster or the galaxy.\* When the convergence is due to an object like a cluster, there is a strong correlation between the convergence  $\kappa_c$  and the shear  $\gamma_c$  that is controlled by the density distribution of the cluster (for our isothermal model  $\kappa_c = \gamma_c$ ). In most circumstances, neglecting the extra surface density coming from nearby objects (galaxies, groups, clusters) leads to an overestimate of the Hubble constant because these objects all have  $\kappa_c > 0$ .

If the cluster is sufficiently close, then we cannot ignore the higher-order perturbations in the expansion of Equation (1.10). They are quantitatively important when they produce deflections at the Einstein ring radius  $b$  of the primary lens,  $B(b/R_c)^2$ , that are larger than the astrometric uncertainties. Because these uncertainties are small, the higher-order terms quickly become important. If they are important but ignored in the models, the results can be very misleading.

## 1.5 Observing Time Delays and Time Delay Lenses

The first time delay measurement, for the gravitational lens Q0957+561, was reported in 1984 (Florentin-Nielsen 1984). Unfortunately, a controversy then developed between a short delay ( $\simeq 1.1$  years, Schild & Cholfin 1986; Vanderriest et al. 1989) and a long delay ( $\simeq 1.5$  years, Press, Rybicki, & Hewitt 1992a,b), which was finally settled in favor of the short delay only after 5 more years of effort (Kundić et al. 1997; also Schild & Thomson 1997 and Haarsma et al. 1999). Factors contributing to the intervening difficulties included the small amplitude of the variations, systematic effects, which, with hindsight, appear to be due to microlensing and scheduling difficulties (both technical and sociological).

While the long-running controversy over Q0957+561 led to poor publicity for the mea-

\* There is a small random component of  $\kappa$  contributed by material along the line of sight (Barkana 1996). This introduces small uncertainties in the  $H_0$  estimates for individual lenses (an rms convergence of 0.01–0.05, depending on the source redshift), but is an unimportant source of uncertainty in estimates from ensembles of lenses because it is a random variable that averages to zero.

\* For the cluster this can be done using weak lensing (e.g., Fischer et al. 1997 in Q0957+561), cluster galaxy velocity dispersions (e.g., Angonin-Willaime, Soucail, & Vanderriest 1994 for Q0957+561, Hjorth et al. 2002 for RXJ0911+0551) or X-ray temperatures/luminosities (e.g., Morgan et al. 2001 for RXJ0911+0551 or Chartas et al. 2002 for Q0957+561). For the lens galaxy this can be done with stellar dynamics (Romanowsky & Kochanek 1999 for Q0957+561 and PG1115+080, Treu & Koopmans 2002b for PG1115+080). The accuracy of these methods is uncertain at present because each suffers from its own systematic uncertainties. When the lens is in the outskirts of a cluster, as in RXJ0911+0551, it is probably reasonable to assume that  $\kappa_c \leq \gamma_c$ , as most mass distributions are more centrally concentrated than isothermal.



Table 1.1. *Time Delay Measurements*

System	$N_{im}$	$\Delta t$ (days)	Astrometry	Model	Ref.
HE1104–1805	2	$161 \pm 7$	+	“simple”	1
PG1115+080	4	$25 \pm 2$	+	“simple”	2
SBS1520+530	2	$130 \pm 3$	+	“simple”	3
B1600+434	2	$51 \pm 2$	+/-	“simple”	4
HE2149–2745	2	$103 \pm 12$	+	“simple”	5
RXJ0911+0551	4	$146 \pm 4$	+	cluster/satellite	6
Q0957+561	2	$417 \pm 3$	+	cluster	7
B1608+656	4	$77 \pm 2$	+/-	satellite	8
B0218+357	2	$10.5 \pm 0.2$	–	“simple”	9
PKS1830–211	2	$26 \pm 4$	–	“simple”	10
B1422+231	4	$(8 \pm 3)$	+	“simple”	11

$N_{im}$  is the number of images.  $\Delta t$  is the longest of the measured delays and its  $1\sigma$  error; delays in parenthesis require further confirmation. The “Astrometry” column indicates the quality of the astrometric data for the system: + (good), +/- (some problems), – (serious problems). The “Model” column indicates the type of model needed to interpret the delays. “Simple” lenses can be modeled as a single primary lens galaxy in a perturbing tidal field. More complex models are needed if there is a satellite galaxy inside the Einstein ring (“satellite”) of the primary lens galaxy, or if the primary lens belongs to a cluster. References: (1) Ofek & Maoz 2003, also see Gil-Merino, Wistozki, & Wambsganss 2002, Pelt, Refsdal, & Stabell 2002, and Schechter et al. 2002; (2) Barkana 1997, based on Schechter et al. 1997; (3) Burud et al. 2002b; (4) Burud et al. 2000, also Koopmans et al. 2000; (5) Burud et al. 2002a; (6) Hjorth et al. 2002; (7) Kundić et al. 1997, also Schild & Thomson 1997 and Haarsma et al. 1999; (8) Fassnacht et al. 2002; (9) Biggs et al. 1999, also Cohen et al. 2000; (10) Lovell et al. 1998; (11) Patnaik & Narasimha 2001.

surement of time delays, it allowed the community to come to an understanding of the systematic problems in measuring time delays, and to develop a broad range of methods for reliably determining time delays from typical data. Only the sociological problem of conducting large monitoring projects remains as an impediment to the measurement of time delays in large numbers. Even these are slowly being overcome, with the result that the last five years have seen the publication of time delays in 11 systems (see Table 1.1).

The basic procedures for measuring a time delay are simple. A monitoring campaign must produce light curves for the individual lensed images that are well sampled compared to the time delays. During this period, the source quasar in the lens must have measurable brightness fluctuations on time scales shorter than the monitoring period. The resulting light curves are cross correlated by one or more methods to measure the delays and their uncertainties (e.g., Press et al. 1992a,b; Beskin & Oknyanskij 1995; Pelt et al. 1996; references in Table 1.1). Care must be taken because there can be sources of uncorrelated variability

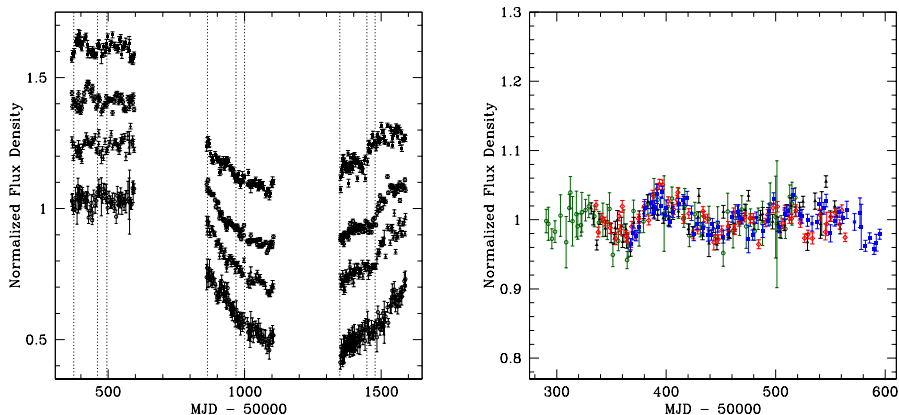


Fig. 1.2. VLA monitoring data for the four-image lens B1608+656. The left panel shows (from top to bottom) the normalized light curves for the B (filled squares), A (open diamonds), C (filled triangles) and D (open circles) images as a function of the mean Julian day. The right panel shows the composite light curve for the first monitoring season after cross correlating the light curves to determine the time delays ( $\Delta t_{AB} = 31.5 \pm 1.5$ ,  $\Delta t_{CB} = 36.0 \pm 1.5$  and  $\Delta t_{DB} = 77.0 \pm 1.5$  days) and the flux ratios. (From Fassnacht et al. 2002.)

ity between the images due to systematic errors in the photometry and real effects such as microlensing of the individual images (e.g., Koopmans et al. 2000; Burud et al. 2002b; Schechter et al. 2003). Figure 1.2 shows an example, the beautiful light curves from the radio lens B1608+656 by Fassnacht et al. (2002), where the variations of all four lensed images have been traced for over three years. One of the 11 systems, B1422+231, is limited by systematic uncertainties in the delay measurements. The brand new time delay for HE1104–1805 (Ofek & Maoz 2003) is probably accurate, but has yet to be interpreted in detail.

We want to have uncertainties in the time delay measurements that are unimportant for the estimates of  $H_0$ . For the present, uncertainties of order 3%–5% are adequate (so improved delays are still needed for PG1115+080, HE2149–2745, and PKS1830–211). In a four-image lens we can measure three independent time delays, and the dimensionless ratios of these delays provide additional constraints on the lens models (see §1.3). These ratios are well measured in B1608+656 (Fassnacht et al. 2002), poorly measured in PG1115+080 (Barkana 1997; Schechter et al. 1997; Chartas 2003) and unmeasured in either RXJ0911+0551 or B1422+231. Using the time delay lenses as very precise probes of  $H_0$ , dark matter and cosmology will eventually require still smaller delay uncertainties ( $\sim 1\%$ ). Once a delay is known to 5%, it is relatively easy to reduce the uncertainties further because we can accurately predict when flux variations will appear in the other images and need to be monitored.

The expression for the time delay in an SIS lens (Eqn. 1.4) reveals the other data that are necessary to interpret time delays. First, the source and lens redshifts are needed to compute the distance factors that set the scale of the time delays. Fortunately, we know both redshifts for all 11 systems in Table 1.1. The dependence of the angular-diameter distances on the

cosmological model is unimportant until our total uncertainties approach 5% (see §1.8). Second, we require accurate relative positions for the images and the lens galaxy. These uncertainties are always dominated by the position of the lens galaxy relative to the images. For most of the lenses in Table 1.1, observations with radio interferometers (VLA, Merlin, VLBA) and *HST* have measured the relative positions of the images and lenses to accuracies  $\lesssim 0''.005$ . Sufficiently deep *HST* images can obtain the necessary data for almost any lens, but dust in the lens galaxy (as seen in B1600+434 and B1608+656) can limit the accuracy of the measurement even in a very deep image. For B0218+357 and PKS1830–211, however, the position of the lens galaxy relative to the images is not known to sufficient precision or is disputed (see Léhar et al. 2000; Courbin et al. 2002; Winn et al. 2002).

In practice, we fit models of the gravitational potential constrained by the available data on the image and lens positions, the relative image fluxes, and the relative time delays. When imposing these constraints, it is important to realize that lens galaxies are not perfectly smooth. They contain both low-mass satellites and stars that perturb the gravitational potential. The time delays themselves are completely unaffected by these substructures. However, as we take derivatives of the potential to determine the ray deflections or the magnification, the sensitivity to substructures in the lens galaxy grows. Models of substructure in cold dark matter (CDM) halos predict that the substructure produces random perturbations of approximately  $0''.001$  in the image positions (see Metcalf & Madau 2001; Dalal & Kochanek 2002). We should not impose tighter astrometric constraints than this limit. A more serious problem is that substructure, whether satellites (“millilensing”) or stars (“microlensing”), significantly affect image fluxes with amplitudes that depend on the image magnification and parity (see, e.g., Wozniak et al. 2000; Burud et al. 2002b; Dalal & Kochanek 2002; Schechter et al. 2003 or Schechter & Wambsganss 2002). Once the flux errors are enlarged to the 30% level of these systematic errors, they provide little leverage for discriminating between models.

We can also divide the systems by the complexity of the required lens model. We define eight of the lenses as “simple,” in the sense that the available data suggests that a model consisting of a single primary lens in a perturbing shear (tidal gravity) field should be an adequate representation of the gravitational potential. In some of these cases, an external potential representing a nearby galaxy or parent group will improve the fits, but the differences between the tidal model and the more complicated perturbing potential are small (see §1.4). We include the quotation marks because the classification is based on an impression of the systems from the available data and models. While we cannot guarantee that a system is simple, we can easily recognize two complications that will require more complex models.

The first complication is that some primary lenses have less massive satellite galaxies inside or near their Einstein rings. This includes two of the time delay lenses, RXJ0911+0551 and B1608+656. RXJ0911+0551 could simply be a projection effect, since neither lens galaxy shows irregular isophotes. Here the implication for models may simply be the need to include all the parameters (mass, position, ellipticity ...) required to describe the second lens galaxy, and with more parameters we would expect greater uncertainties in  $H_0$ . In B1608+656, however, the lens galaxies show the heavily disturbed isophotes typical of galaxies undergoing a disruptive interaction. How one should model such a system is unclear. If there was once dark matter associated with each of the galaxies, how is it distributed now? Is it still associated with the individual galaxies? Has it settled into an equilibrium

configuration? While B1608+656 can be well fit with standard lens models (Fassnacht et al. 2002), these complications have yet to be explored.

The second complication occurs when the primary lens is a member of a more massive (X-ray) cluster, as in the time delay lenses RXJ0911+0551 (Morgan et al. 2001) and Q0957+561 (Chartas et al. 2002). The cluster model is critical to interpreting these systems (see §1.4). The cluster surface density at the position of the lens ( $\kappa_c \gtrsim 0.2$ ) leads to large corrections to the time delay estimates and the higher-order perturbations are crucial to obtaining a good model. For example, models in which the Q0957+561 cluster was treated simply as an external shear are grossly incorrect (see the review of Q0957+561 models in Keeton et al. 2000). In addition to the uncertainties in the cluster model itself, we must also decide how to include and model the other cluster galaxies near the primary lens. Thus, lenses in clusters have many reasonable degrees of freedom beyond those of the “simple” lenses.

## 1.6 Results: The Hubble Constant and Dark Matter

With our understanding of the theory and observations of the lenses we will now explore their implications for  $H_0$ . We focus on the “simple” lenses PG1115+080, SBS1520+530, B1600+434, and HE2149–2745. We only comment on the interpretation of the HE1104–1805 delay because the measurement is too recent to have been interpreted carefully. We will briefly discuss the more complicated systems RXJ0911+0551, Q0957+561, and B1608+656, and we will not discuss the systems with problematic time delays or astrometry.

The most common, simple, realistic model of a lens consists of a singular isothermal ellipsoid (SIE) in an external (tidal) shear field (Keeton et al. 1997). The model has 7 parameters (the lens position, mass, ellipticity, major axis orientation for the SIE, and the shear amplitude and orientation). It has many degrees of freedom associated with the angular structure of the potential, but the radial structure is fixed with  $\langle \kappa \rangle \simeq 1/2$ . For comparison, a two-image (four-image) lens supplies 5 (13) constraints on any model of the potential: 2 (6) from the relative positions of the images, 1 (3) from the flux ratios of the images, 0 (2) from the inter-image time delay ratios, and 2 from the lens position. With the addition of extra components (satellites/clusters) for the more complex lenses, this basic model provides a good fit to all the time delay lenses except Q0957+561. Although a naive counting of the degrees of freedom ( $N_{dof} = -2$  and 6, respectively) suggests that estimates of  $H_0$  would be underconstrained for two-image lenses and overconstrained for four-image lenses, the uncertainties are actually dominated by those of the time delay measurements and the astrometry in both cases. This is what we expect from §1.3 — the model has no degrees of freedom that change  $\langle \kappa \rangle$  or  $\eta$ , so there will be little contribution to the uncertainties in  $H_0$  from the model for the potential.

If we use a model that includes parameters to control the radial density profile (i.e.,  $\langle \kappa \rangle$ ), for example by adding a halo truncation radius  $a$  to the SIS profile [the pseudo-Jaffe model,  $\rho \propto r^{-2}(r^2 + a^2)^{-1}$ ; e.g., Impey et al. 1998; Burud et al. 2002a],\* then we find the expected correlation between  $a$  and  $H_0$  — as we make the halo more concentrated (smaller  $a$ ), the estimate of  $H_0$  rises from the value for the SIS profile ( $\langle \kappa \rangle = 1/2$  as  $a \rightarrow \infty$ ) to the value for a point mass ( $\langle \kappa \rangle = 0$  as  $a \rightarrow 0$ ), with the fastest changes occurring when  $a$  is similar to the Einstein radius of the lens. We show an example of such a model for PG1115+080 in Figure 1.3. This case is somewhat more complicated than a pure pseudo-Jaffe model because

\* This is simply an example. The same behavior would be seen for any other parametric model in which the radial density profile can be adjusted.

there is an additional contribution to the surface density from the group to which the lens galaxy belongs. As long as the structure of the radial density profile is fixed (constant  $a$ ), the uncertainties are again dominated by the uncertainties in the time delay. Unfortunately, the goodness of fit,  $\chi^2(a)$ , shows too little dependence on  $a$  to determine  $H_0$  uniquely. In general, two-image lenses have too few constraints, and the extra constraints supplied by a four-image lens constrain the angular structure rather than the radial structure of the potential. This basic problem holds for all existing models of the current sample of time delay lenses.

The inability of the present time delay lenses to directly constrain the radial density profile is the major problem for using them to determine  $H_0$ . Fortunately, it is a consequence of the available data on the current sample rather than a fundamental limitation, as we discuss in the next section (§1.7). It is, however, a simple trade-off – models with less dark matter (lower  $\langle\kappa\rangle$ , more centrally concentrated densities) produce higher Hubble constants than those with more dark matter. We do have some theoretical limits on the value of  $\langle\kappa\rangle$ . In particular, we can be confident that the surface density is bounded by two limiting models. The mass distribution should not be more compact than the luminosity distribution, so a constant mass-to-light ratio ( $M/L$ ) model should set a lower limit on  $\langle\kappa\rangle \gtrsim \langle\kappa\rangle_{M/L} \simeq 0.2$ , and an upper limit on estimates of  $H_0$ . We are also confident that the typical lens should not have a rising rotation curve at 1–2 optical effective radii from the center of the lens galaxy. Thus, the SIS model is probably the least concentrated reasonable model, setting an upper bound on  $\langle\kappa\rangle \lesssim \langle\kappa\rangle_{SIS} = 1/2$ , and a lower limit on estimates of  $H_0$ . Figure 1.4 shows joint estimates of  $H_0$  from the four simple lenses for these two limiting mass distributions (Kochanek 2003b). The results for the individual lenses are mutually consistent and are unchanged by the new  $0.149 \pm 0.004$  day delay for the  $A_1$ - $A_2$  images in PG1115+080 (Chartas 2003). For galaxies with isothermal profiles we find  $H_0 = 48 \pm 3 \text{ km s}^{-1} \text{ Mpc}^{-1}$ , and for galaxies with constant  $M/L$  we find  $H_0 = 71 \pm 3 \text{ km s}^{-1} \text{ Mpc}^{-1}$ . While our best prior estimate for the mass distribution is the isothermal profile (see §1.7), the lens galaxies would have to have constant  $M/L$  to match Key Project estimate of  $H_0 = 72 \pm 8 \text{ km s}^{-1} \text{ Mpc}^{-1}$  (Freedman et al. 2001).

The difference between these two limits is entirely explained by the differences in  $\langle\kappa\rangle$  and  $\eta$  between the SIS and constant  $M/L$  models. In fact, it is possible to reduce the  $H_0$  estimates for each simple lens to an approximation formula,  $H_0 = A(1 - \langle\kappa\rangle) + B\langle\kappa\rangle(\eta - 1)$ . The coefficients,  $A$  and  $|B| \approx A/10$ , are derived from the image positions using the simple theory from §1.3. These approximations reproduce numerical results using ellipsoidal lens models to accuracies of  $3 \text{ km s}^{-1} \text{ Mpc}^{-1}$  (Kochanek 2002). For example, in Figure 1.3 we also show the estimate of  $H_0$  computed based on the simple theory of §1.3 and the annular surface density ( $\langle\kappa\rangle$ ) and slope ( $\eta$ ) of the numerical models. The agreement with the full numerical solutions is excellent, even though the numerical models include both the ellipsoidal lens galaxy and a group. No matter what the mass distribution is, the five lenses PG1115+080, SBS1520+530, B1600+434, PKS1830–211,\* and HE2149–2745 have very similar dark matter halos. For a fixed slope  $\eta$ , the five systems are consistent with a common value for the surface density of

$$\langle\kappa\rangle = 1 - 1.07h + 0.14(\eta - 1)(1 - h) \pm 0.04 \quad (1.11)$$

\* PKS1830–211 is included based on the Winn et al. (2002) model of the *HST* imaging data as a single lens galaxy. Courbin et al. (2002) prefer an interpretation with multiple lens galaxies which would invalidate the analysis.

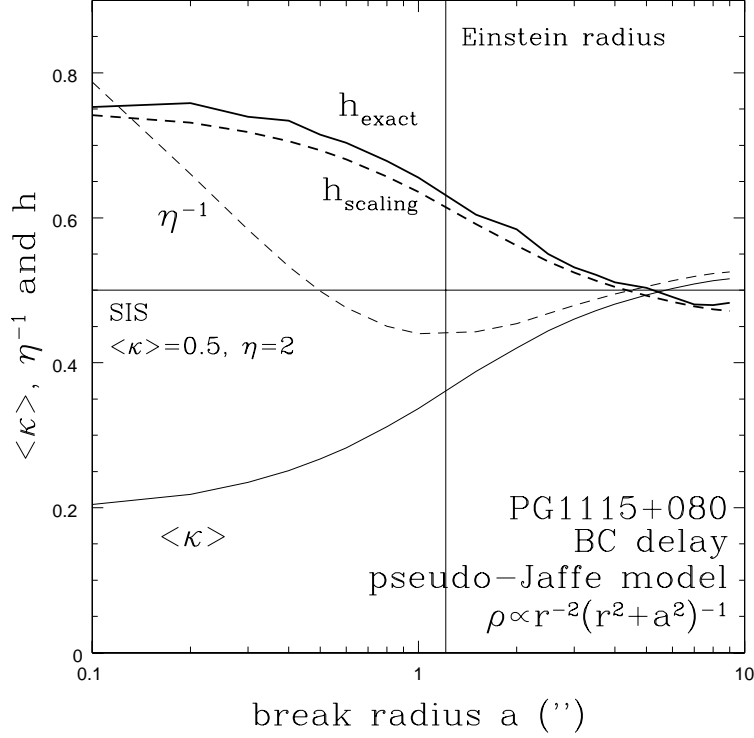


Fig. 1.3.  $H_0$  estimates for PG1115+080. The lens galaxy is modeled as a ellipsoidal pseudo-Jaffe model,  $\rho \propto r^{-2}(r^2 + a^2)^{-1}$ , and the nearby group is modeled as an SIS. As the break radius  $a \rightarrow \infty$  the pseudo-Jaffe model becomes an SIS model, and as the break radius  $a \rightarrow 0$  it becomes a point mass. The heavy solid curve ( $h_{exact}$ ) shows the dependence of  $H_0$  on the break radius for the exact, nonlinear fits of the model to the PG1115+080 data. The heavy dashed curve ( $h_{scaling}$ ) is the value found using our simple theory (§1.3) of time delays. The agreement of the exact and scaling solutions is typical. The light solid line shows the average surface density  $\langle \kappa \rangle$  in the annulus between the images, and the light dashed line shows the *inverse* of the logarithmic slope  $\eta$  in the annulus. For an SIS model we would have  $\langle \kappa \rangle = 1/2$  and  $\eta^{-1} = 1/2$ , as shown by the horizontal line. When the break radius is large compared to the Einstein radius (indicated by the vertical line), the surface density is slightly higher and the slope is slightly shallower than for the SIS model because of the added surface density from the group. As we make the lens galaxy more compact by reducing the break radius, the surface density decreases and the slope becomes steeper, leading to a rise in  $H_0$ . As the galaxy becomes very compact, the surface density near the Einstein ring is dominated by the group rather than the galaxy, so the surface density approaches a constant and the logarithmic slope approaches the value corresponding to a constant density sheet ( $\eta = 1$ ).

where  $H_0 = 100h \text{ km s}^{-1} \text{ Mpc}^{-1}$  and there is an upper limit of  $\sigma_\kappa \lesssim 0.07$  on the intrinsic scatter of  $\langle \kappa \rangle$ . Thus, time delay lenses provide a new window into the structure and homogeneity of dark matter halos, regardless of the actual value of  $H_0$ .

There is an enormous range of parametric models that can illustrate how the extent of the halo affects  $\langle \kappa \rangle$  and hence  $H_0$  — the pseudo-Jaffe model we used above is only one

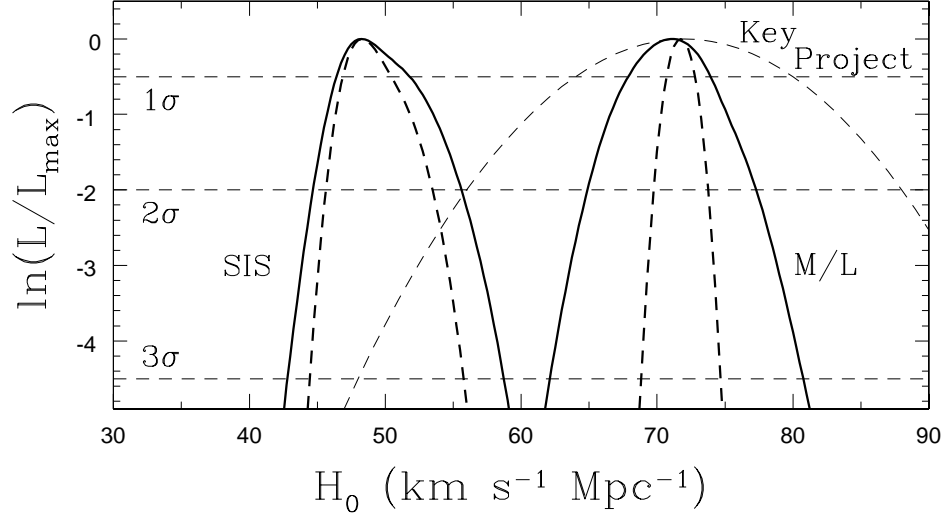


Fig. 1.4.  $H_0$  likelihood distributions. The curves show the joint likelihood functions for  $H_0$  using the four simple lenses PG1115+080, SBS1520+530, B1600+434, and HE2149–2745 and assuming either an SIS model (high  $\langle\kappa\rangle$ , flat rotation curve) or a constant  $M/L$  model (low  $\langle\kappa\rangle$ , declining rotation curve). The heavy dashed curves show the consequence of including the X-ray time delay for PG1115+080 from Chartas (2003) in the models. The light dashed curve shows a Gaussian model for the Key Project result that  $H_0 = 72 \pm 8 \text{ km s}^{-1} \text{ Mpc}^{-1}$ .

example. It is useful, however, to use a physically motivated model where the lens galaxy is embedded in a standard NFW (Navarro, Frenk, & White 1996) profile halo. The lens galaxy consists of the baryons that have cooled to form stars, so the mass of the visible galaxy can be parameterized using the cold baryon fraction  $f_{b,cold}$  of the halo, and for these CDM halo models the value of  $\langle\kappa\rangle$  is controlled by the cold baryon fraction (Kochanek 2003a). A constant  $M/L$  model is the limit  $f_{b,cold} \rightarrow 1$  (with  $\langle\kappa\rangle \simeq 0.2$ ,  $\eta \simeq 3$ ). Since the baryonic mass fraction of a CDM halo should not exceed the global fraction of  $f_b \simeq 0.15 \pm 0.05$  (e.g., Wang, Tegmark, & Zaldarriaga 2002), we cannot use constant  $M/L$  models without also abandoning CDM. As we reduce  $f_{b,cold}$ , we are adding mass to an extended halo around the lens, leading to an increase in  $\langle\kappa\rangle$  and a decrease in  $\eta$ . For  $f_{b,cold} \simeq 0.02$  the model closely resembles the SIS model ( $\langle\kappa\rangle \simeq 1/2$ ,  $\eta \simeq 2$ ). If we reduce  $f_{b,cold}$  further, the mass distribution begins to approach that of the NFW halo without any cold baryons. Figure 1.5 shows how  $\langle\kappa\rangle$  and  $H_0$  depend on  $f_{b,cold}$  for PG1115+080, SBS1520+530, B1600+434 and HE2149–2745. When  $f_{b,cold} \simeq 0.02$ , the CDM models have parameters very similar to the SIS model, and we obtain a very similar estimate of  $H_0 = 52 \pm 6 \text{ km s}^{-1} \text{ Mpc}^{-1}$  (95% confidence). If all baryons cool, and  $f_{b,cold} = f_b$ , then we obtain  $H_0 = 65 \pm 6 \text{ km s}^{-1} \text{ Mpc}^{-1}$  (95% confidence), which is still lower than the Key Project estimates.

We excluded the lenses requiring significantly more complicated models with multiple lens galaxies or very strong perturbations from clusters. If we have yet to reach a consensus on the mass distribution of relatively isolated lenses, it seems premature to extend the dis-

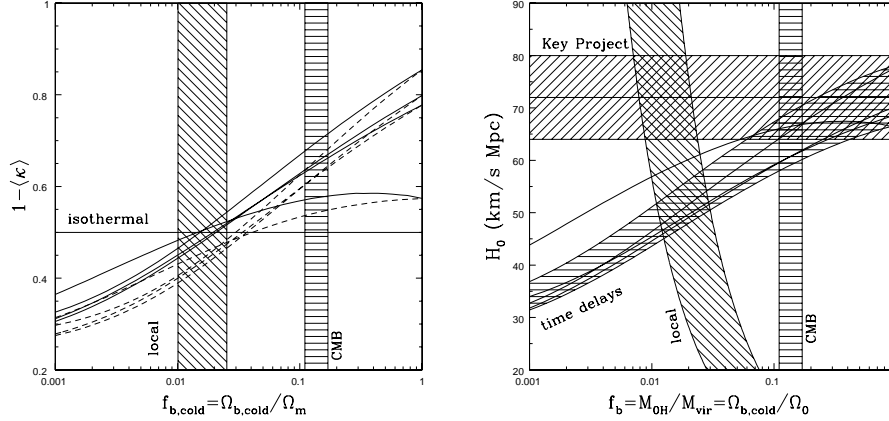


Fig. 1.5.  $H_0$  in CDM halo models. The left panel shows  $1 - \langle \kappa \rangle$  for the “simple” lenses (PG1115+080, SBS1520+530, B1600+434, and HE2149–2745) as a function of the cold baryon fraction  $f_{b,cold}$ . The solid (dashed) curves include (exclude) the adiabatic compression of the dark matter by the baryons. The horizontal line shows the value for an SIS potential. The right panel shows the resulting estimates of  $H_0$ , where the shaded envelope bracketing the curves is the 95% confidence region for the combined lens sample. The horizontal band shows the Key Project estimate. For larger  $f_{b,cold}$ , the density  $\langle \kappa \rangle$  decreases and the local slope  $\eta$  steepens, leading to larger values of  $H_0$ . The vertical bands in the two panels show the lower bound on  $f_b$  from local inventories and the upper bound from the CMB.

cussion to still more complicated systems. We can, however, show that the clusters lenses require significant contributions to  $\langle \kappa \rangle$  from the cluster in order to produce the same  $H_0$  as the more isolated systems. As we discussed in §1.5 the three more complex systems are RXJ0911+0551, Q0957+561 and B1608+656.

RXJ0911+0551 is very strongly perturbed by the nearby X-ray cluster (Morgan et al. 2001; Hjorth et al. 2002). Kochanek (2003b) found  $H_0 = 49 \pm 5 \text{ km s}^{-1} \text{ Mpc}^{-1}$  if the primary lens and its satellite were isothermal and  $H_0 = 67 \pm 5 \text{ km s}^{-1} \text{ Mpc}^{-1}$  if they had constant mass-to-light ratios. The higher value of  $H_0 = 71 \pm 4 \text{ km s}^{-1} \text{ Mpc}^{-1}$  obtained by Hjorth et al. (2002) can be understood by combining §1.3 and §1.4 with the differences in the models. In particular, Hjorth et al. (2002) truncated the halo of the primary lens near the Einstein radius and used a lower mass cluster, both of which lower  $\langle \kappa \rangle$  and raise  $H_0$ . The Hjorth et al. (2002) models also included many more cluster galaxies assuming fixed masses and halo sizes.

Q0957+561 is a special case because the primary lens galaxy is the brightest cluster galaxy and it lies nearly at the cluster center (Keeton et al. 2000; Chartas et al. 2002). As a result, the lens modeling problems are particularly severe, and Keeton et al. (2000) found that all previous models (most recently, Barkana et al. 1999; Bernstein & Fischer 1999; and Chae 1999) were incompatible with the observed geometry of the lensed host galaxy. While Keeton et al. (2000) found models consistent with the structure of the lensed host, they covered a range of almost  $\pm 25\%$  in their estimates of  $H_0$ . A satisfactory treatment of this lens remains elusive.

HE1104–1805 had its delay measured (Ofek & Maoz 2003) just as we completed this



review. Assuming the  $\Delta t = 161 \pm 7$  day delay is correct, a standard SIE model of this system predicts a very high  $H_0 \simeq 90 \text{ km s}^{-1} \text{ Mpc}^{-1}$ . The geometry of this system and the fact that the inner image is brighter than the outer image both suggest that HE1104–1805 lies in an anomalously high tidal shear field, while the standard model includes a prior to keep the external shear small. A prior is needed because a two-image lens supplies too few constraints to determine both the ellipticity of the main lens and the external shear simultaneously. Since the images and the lens in HE1104–1805 are nearly colinear, the anomalous  $H_0$  estimate for the standard model may be an example of the shear degeneracy we briefly mentioned in §1.3. At present the model surveys needed to understand the new delay have not been made. Observations of the geometry of the host galaxy Einstein ring will resolve any ambiguities due to the shear in the near future (see §1.7).

The lens B1608+656 consists of two interacting galaxies, and, as we discussed in §1.5, this leads to a greatly increased parameter space. Fassnacht et al. (2002) used SIE models for the two galaxies to find  $H_0 = 61 - 65 \text{ km s}^{-1} \text{ Mpc}^{-1}$ , depending on whether the lens galaxy positions are taken from the  $H$ -band or  $I$ -band lens *HST* images (the statistical errors are negligible). The position differences are probably created by extinction effects from the dust in the lens galaxies. Like isothermal models of the “simple” lenses, the  $H_0$  estimate is below local values, but the disagreement is smaller. These models correctly match the observed time delay ratios.

## **1.7 Solving the Central Concentration Problem**

We can take four approaches to solving the central concentration problem. First, the density profiles of galaxies are not a complete mystery, and we could apply the constraints derived from observations of other (early-type) galaxies to the time delay systems. Second, we could make new observations of the existing time delay lenses in order to obtain additional data that would constrain the density profiles. Third, we could measure the time delays in the systems where the lens galaxies already have well-constrained densities. Fourth, we can use the statistical properties of time delay lenses to break the degeneracies seen in individual lenses.

If we assume that the time delay lenses have the same density structure as other early-type galaxies, then models close to isothermal are favored. For lenses with extended or multi-component sources, the lens models constrain the density distributions and the best fit models are usually very close to isothermal (e.g., Cohn et al. 2001; Winn, Rusin, & Kochanek 2003). Stellar dynamical observations of lenses also favor isothermal models (e.g., Treu & Koopmans 2002a). Stellar dynamical (e.g., Romanowsky & Kochanek 1999; Gerhard et al. 2001) and X-ray (e.g., Loewenstein & Mushotzky 2003) observations of nearby early-type galaxies generally find flat rotation curves on the relevant scales. Finally, weak lensing analyses require significant dark matter on large scales in early-type galaxies (McKay et al. 2002). In general, the data on early-type galaxies seem to prefer isothermal models on the scales relevant to interpreting time delays, while constant  $M/L$  models are firmly ruled out. If we must ultimately rely on the assumption that the density profiles of time delay lenses are similar to those of other early-type galaxies, the additional uncertainty added by this assumption will be small and calculable. Moreover, the assumption is no different from the assumptions of homogeneity used in other studies of the distance scale.

We can avoid any such assumptions by determining the density profiles of the time delay lenses directly. One approach is to measure the kinematic properties of the lens galaxy. Since

the mass inside the Einstein ring is fixed by the image geometry, the velocity dispersion is controlled by the central concentration of the density. Treu & Koopmans (2002b) apply this method to PG1115+080 and argue that the observed velocity dispersion requires a mass distribution between the isothermal and constant  $M/L$  limits with  $H_0 = 59_{-7}^{+12}$  km s<sup>-1</sup> Mpc<sup>-1</sup>. Note, however, that with this velocity dispersion the lens galaxy does not lie on the fundamental plane, which is very peculiar. A second approach is to use deep infrared imaging to determine the structure of the lensed host galaxy of the quasar (Kochanek, Keeton, & McLeod 2001). The location and width of the Einstein ring depends on both the radial and angular structure of the potential, although the sensitivity to the radial structure of the lens is weak when the annulus bracketing the lensed images is thin ( $\Delta R/\langle R \rangle$  small; Saha & Williams 2001). This method will work best for asymmetric two-image lenses ( $\Delta R/\langle R \rangle \approx 1$ ). The necessary data can be obtained with *HST* for most time delay lenses.

We can also focus our monitoring campaigns on lenses already known to have well-constrained density profiles. For the reasons we have already discussed, systems with multi-component sources, well-studied images of the host galaxy or stellar dynamical measurements will have better constrained density profiles than those without any additional constraints. We can also avoid most of the uncertainties in the density profile by measuring the time delays of very low-redshift lenses. When the lens is very close to the observer, the images lie very close to the center of the lens where the stellar mass dominates. A constant  $M/L$  model then becomes a very good approximation and we need worry little about the amount or the distribution of the dark matter. The one such candidate at present, Q2237+0305 at  $z_l = 0.04$ , will have very short delays, but these could be measured by an X-ray monitoring program using the *Chandra* observatory.

Finally, the statistical properties of larger samples of time delay lenses will also help to solve the problem. We already saw in §1.6 that the “simple” time delay lenses must have very similar densities, independent of  $H_0$ . This already means that the implications for  $H_0$  no longer depend on individual lenses. In some ways the similarity of the densities is not an advantage — it is actually easier to determine  $H_0$  if the density distributions are inhomogeneous (Kochanek 2003b). On the other hand, there are well-defined approaches to using the statistical properties of lens models to estimate parameters that cannot be determined from the models of the individual systems (see Kochanek 2001). The statistics of the problematic flux ratios observed in the lenses (see §1.5) may also provide a means of estimating  $\langle \kappa \rangle$ . Schechter & Wambsganss (2002) point out that in four-image quasar lenses there is a tendency for the brightest saddle point image to be demagnified compared to reasonable lens models. Microlensing by the stars can naturally explain the observations if the surface density of stars is a small fraction of the total surface density near the images ( $\kappa_* \ll \langle \kappa \rangle$ ), which would rule out constant  $M/L$  models where  $\kappa_* \simeq \langle \kappa \rangle$ .

## 1.8 Conclusions

The determination of  $H_0$  using gravitational lens time delays has come of age. The last few years have seen a dramatic increase in the number of delay measurements, and there is no barrier other than sociology to rapidly increasing the sample. The interpretation of time delays requires a model for the gravitational potential of the lens. Fortunately, the physics determining time delays is well understood, and the only important variable is the average surface density  $\langle \kappa \rangle$  of the lens near the images for which the delay is measured. Unfortunately, there is a tendency in the literature to conceal rather than to illuminate this

understanding. Provided a lens does not lie in a cluster where the cluster potential cannot be described by a simple expansion, any lens model that includes the parameters needed to vary the average surface density of the lens near the images and to change the ratio between the quadrupole moment of the lens and the environment includes all the parameters needed to model time delays, to estimate the Hubble constant, and to understand the systematic uncertainties in the results. *All differences between estimates of the Hubble constant for the simple time delay lenses can be understood on this basis.*

Models for the four time delay lenses that can be modeled using a single lens galaxy predict that  $H_0 = 48 \pm 3 \text{ km s}^{-1} \text{ Mpc}^{-1}$  if the lens galaxies have isothermal density profiles with flat rotation curves, and  $H_0 = 71 \pm 3 \text{ km s}^{-1} \text{ Mpc}^{-1}$  if they have constant mass-to-light ratios. The Key Project estimate of  $H_0 = 72 \pm 8 \text{ km s}^{-1} \text{ Mpc}^{-1}$  agrees with the lensing results only if the lenses have little dark matter. We have strong theoretical prejudices and estimates from other observations of early-type galaxies that we should favor the isothermal models over the constant  $M/L$  models. We feel that we have reached the point where the results from gravitational lens time delays deserve serious attention and that there is a reasonable likelihood that the local estimates of  $H_0$  are too high. A modest investment of telescope time would allow the measurement of roughly 5–10 time delays per year, and these new delays would rapidly test the current results. Other observations of time delay lenses to measure the velocity dispersions of the lens galaxies or to determine the geometry of the lensed images of the quasar host galaxy can be used to constrain the mass distributions directly. The systematic problems associated with the density profile are soluble not only in theory but also in practice, and the investment of the community's resources would be significantly less than already invested in the distance scale.

The time delay measurements also provide a new probe of the density structure of galaxies at the boundary between the baryonic and dark matter dominated parts of galaxies (projected distances of 1–2 effective radii). Even if we ignore the actual value of  $H_0$ , we can still study the differences in the surface densities. For example, we can show that the present sample of simple lenses must have very similar surface densities. This region is very difficult to study with other probes.

Finally, the time delay measurements can be used to determine cosmological parameters. Time delays basically measure the distance to the lens galaxy, so we can make the same sorts of cosmological measurements as Type Ia supernovae. If the variations in  $\langle \kappa \rangle$  between lens galaxies are small, as seem to be indicated by the present data, then the accuracy of the differential measurements will be very good. The present sample has little sensitivity to the cosmological model even with the mass distribution fixed because the time delay uncertainties are still too large and the redshift range is too restricted ( $z_l = 0.31$  to  $0.72$ ). If we assume that other methods will determine the distance factors more accurately and rapidly, then we can use the time delays to study the evolution of galaxy mass distributions with redshift.

**Acknowledgements.** CSK thanks D. Rusin and J. Winn for their comments. CSK is supported by the Smithsonian Institution and NASA ATP grant NAG5-9265.

## References

Angonin-Willaime, M.-C., Soucail, G., & Vandriest, C. 1994, A&A, 291, 411

*C. S. Kochanek and P. L. Schechter*

- Barkana, R. 1996, *ApJ*, 468, 17  
———. 1997, *ApJ*, 489, 21  
Barkana, R., Lehár, J., Falco, E. E., Grogin, N. A., Keeton, C. R., & Shapiro, I. I. 1999, *ApJ*, 520, 479  
Bernstein, G., & Fischer, P. 1999, *AJ*, 118, 14  
Beskin, G. M., & Oknyanskij, V. L. 1995, *A&A*, 304, 341  
Biggs, A. D., Browne, I. W. A., Helbig, P., Koopmans, L. V. E., Wilkinson, P. N., & Perley, R. A. 1999, *MNRAS*, 304, 349  
Blandford, R. D., & Narayan, R. 1987, *ApJ*, 310, 568  
Bullock, J. S., Kolatt, T. S., Sigad, Y., Somerville, R. S., Kravtsov, A. V., Klypin, A. A., Primack, J. R., & Dekel, A. 2001, *MNRAS*, 321, 559  
Burud, I., et al. 2000, *ApJ*, 544, 117  
———. 2002a, *A&A*, 383, 71  
———. 2002b, *A&A*, 391, 481  
Chae, K.-H. 1999, *ApJ*, 524, 582  
Chartas, G. 2003, *Carnegie Observatories Astrophysics Series, Vol. 2: Measuring and Modeling the Universe*, ed. W. L. Freedman (Pasadena: Carnegie Observatories,  
<http://www.ociw.edu/ociw/symposia/series/symposium2/proceedings.html>)  
Chartas, G., Gupta, V., Garmire, G., Jones, C., Falco, E. E., Shapiro, I. I., & Tavecchio, F. 2002, *ApJ*, 565, 96  
Cohen, A. S., Hewitt, J. N., Moore, C. B., & Haarsma, D. B. 2000, *ApJ*, 545, 578  
Cohn, J. D., Kochanek, C. S., McLeod, B. A., & Keeton, C. R. 2001, *ApJ*, 554, 1216  
Courbin, F., Meylan, G., Kneib, J.-P., & Lidman, C. 2002, *ApJ*, 575, 95  
Dalal, N., & Kochanek, C. S. 2002, *ApJ*, 572, 25  
Fassnacht, C. D., Xanthopoulos, E., Koopmans, L. V. E., & Rusin, D. 2002, *ApJ*, 581, 823  
Falco, E. E., Gorenstein, M. V., & Shapiro, I. I. 1985, *ApJ*, 289, L1  
Fischer, P., Bernstein, G., Rhee, G., & Tyson, J. A. 1997, *AJ*, 113, 521  
Florentin-Nielsen, R. 1984, *A&A*, 138, L19  
Freedman, W. L., et al. 2001, *ApJ*, 553, 47  
Gerhard, O., Kronawitter, A., Saglia, R. P., & Bender, R. 2001, *AJ*, 121, 1936  
Gil-Merino, R., Wisotzki, L., & Wambsganss, J. 2002, *A&A*, 381, 428  
Gorenstein, M. V., Falco, E. E., & Shapiro, I. I. 1988, *ApJ*, 327, 693  
Haarsma, D. B., Hewitt, J. N., Lehár, J., & Burke, B. F. 1999, *AJ*, 510, 64  
Hjorth, J., et al., 2002, *ApJ*, 572, L11  
Impey, C. D., Falco, E. E., Kochanek, C. S., Lehár, J., McLeod, B. A., Rix, H.-W., Peng, C. Y., & Keeton, C. R. 1998, *ApJ*, 509, 551  
Keeton, C. R., et al. 2000, *ApJ*, 542, 74  
Keeton, C. R. 2003, *ApJ*, submitted (astro-ph/0102340)  
Keeton, C. R., Kochanek, C. S., & Seljak, U. 1997, *ApJ*, 482, 604  
Kochanek, C. S. 2001, in *The Shapes of Galaxies and Their Dark Halos*, ed. P. Natarajan (Singapore: World Scientific), 62  
———. 2002, *ApJ*, 578, 25  
———. 2003a, *ApJ*, 583, 49  
———. 2003b, astro-ph/0204043  
Kochanek, C. S., Keeton, C. R., & McLeod, B. A. 2001, *ApJ*, 547, 50  
Koopmans, L. V. E., de Bruyn, A. G., Xanthopoulos, E., & Fassnacht, C. D. 2000, *A&A*, 356, 391  
Kundić, T., et al. 1997, *ApJ*, 482, 75  
Lehár, J., et al. 2000, *ApJ*, 536, 584  
Lovell, J. E. J., Jauncey, D. L., Reynolds, J. E., Wieringa, M. H., King, E. A., Tzioumis, A. K., McCulloch, P. M., & Edwards, P. G. 1998, *ApJ*, 508, L51  
Loewenstein, M., & Mushotzky, R. F. 2003, *ApJ*, submitted  
McKay, T. A., et al. 2002, *ApJ*, 571, L85  
Metcalf, R. B., & Madau, P. 2001, *ApJ*, 563, 9  
Morgan, N. D., Chartas, G., Malm, M., Bautz, M. W., Burud, I., Hjorth, J., Jones, S. E., & Schechter, P. L. 2001, *ApJ*, 555, 1  
Narayan, R., & Bartelmann, M. 1999, in *Formation and Structure in the Universe*, ed. A. Dekel & J. P. Ostriker (Cambridge: Cambridge Univ. Press), 360  
Navarro, J. F., Frenk, C. S., & White, S. D. M. 1996, *ApJ*, 462, 563  
Ofek, E. O., & Maoz, D. 2003, *ApJ*, in press

*C. S. Kochanek and P. L. Schechter*

- Patnaik, A. R., & Narasimha, D. 2001, MNRAS, 326, 1403  
Pelt, J., Kayser, R., Refsdal, S., & Schramm, T. 1996, A&A, 305, 97  
Pelt, J., Refsdal, S., & Stabell, R. 2002, A&A, 289, L57  
Press, W. H., Rybicki, G. B., & Hewitt, J. N. 1992a, ApJ, 385, 404  
———. 1992b, ApJ, 385, 416  
Refsdal, S. 1964, 128, 307  
Romanowsky, A. J., & Kochanek, C. S. 1999, ApJ, 516, 18  
Saha, P. 2000, AJ, 120, 1654  
Saha, P., & Williams, L. L. R. 2001, AJ, 122, 585  
Schechter, P. L., et al. 1997, ApJ, 475, L85  
———. 2003, ApJ, 584, 657  
Schechter, P. L., & Wambsganss, J. 2002, ApJ, 580, 685  
Schild, R., & Cholfin, B. 1986, ApJ, 300, 209  
Schild, R., & Thomson, D. J. 1997, AJ, 113, 130  
Schneider, P., Ehlers, J., & Falco, E. E. 1992, Gravitational Lenses, (Berlin: Springer-Verlag)  
Treu, T., & Koopmans, L. V. E. 2002a, ApJ, 568, L5  
———. 2002b, MNRAS, 337, 6  
Vanderriest, C., Schneider, J., Herpe, G., Chevreton, M., Moles, M., & Wlerick, G. 1989, A&A, 215, 1  
Wang, X., Tegmark, M., & Zaldarriaga, M. 2002, Phys. Rev. D, 65, 123001  
Williams, L. L. R., & Saha, P. 2000, AJ, 199, 439  
Winn, J. N., Kochanek, C. S., McLeod, B. A., Falco, E. E., Impey, C. D., & Rix, H.-W. 2002, ApJ, 575, 103  
Winn, J. N., Rusin, D., & Kochanek, C. S. 2003, ApJ, 587, 80  
Witt, H. J., Mao, S., & Keeton, C. R. 2000, ApJ, 544, 98  
Wozniak, P. R., Udalski, A., Szymanski, M., Kubiak, M., Pietrzynski, G., Soszynski, I., & Zebrun, K. 2000, ApJ, 540, L65  
Zhao, H., & Qin, B. 2003a, ApJ, 582, 2  
———. 2003b, ApJ, submitted (astro-ph/0209304)